16

Multi-Stage Peel Tests and Evaluation of Interfacial Adhesion Strength for Micro- and Opto-Electronic Materials

Masaki Omiya, Kikuo Kishimoto, and Wei Yang

Tokyo Institute of Technology, Graduate School of Science and Engineering, Department of Mechanical and Control Engineering 2-12-1, O-okayama, Meguro-ku, Tokyo 152-8552, Japan

16.1. INTRODUCTION

Rapidly development of the electronic products requires small, high density and functional devices. Many layers deposited on silicon substrate can accomplish several kinds of functions in one package. Moreover, in these days, 3-dimensional packaging and assembling technologies have been developing all over the world (e.g., [1]). Multi-layer technology is a key for developing electronic products in future.

The ensuring of reliability is the one of the critical issues in micro- and opto-electronic devices. Those electronic devices contain several kinds of metal or polymer thin films. Due to intrinsic/thermal residual stresses in films or substrates, or elastic/lattice mismatch between film and substrate, the delaminations between layers sometimes occur. The debonding between layers brings about the failure of devices and it might be the source of a tragic accident, since, nowadays, the electronic devices are closely related to human life. One need to design those devices to work well through its entire life time and the information of interfacial strength is essential to designing the reliable devices. Therefore, it is important to evaluate the interfacial strength precisely and the development of reliable testing methods for evaluating the interfacial strength is needed.

Meanwhile, attention has been directed to an electrically conductive ceramic film, which is deposited on a polymeric substrate [2–4]. The applications of those conductive films are used for the display of mobile computers, cellular phones or the flexible paper type display. Those conductive films have the advantage of low power consumption or flexibility to deformation. The popular components of those films especially for the display use are ITO (indium tin oxide) and PET (poly(ethylene terephthalate)). It is well known that the mechanical properties of polymers, such as tensile strength or rupture strain, are degraded by the irradiation of ultraviolet (UV) rays [5]. When the polymer-based conductive films are

used in the open air, it is necessary to consider the degradation of the mechanical properties in designing of such products. The bonding mechanism between ceramic and polymer is mainly intermolecular force. When UV rays irradiate polymeric materials, the principal chains are broken down and oxidized. Those reactions may affect the bonding strength between ceramics and polymers.

In view of interface mechanics, interfacial strength depends on the phase angle of loading. To assess the interface strength, one need to conduct the interfacial fracture tests under a wide range of phase angle. A lot of researches related to the interfacial fracture tests have been published and a detailed review of the appropriate mechanics has been given by Hutchinson and Suo [6], Evans and Hutchinson [7], Evans et al. [8].

Especially for the adhesion strength of thin films on substrates, the conventional methods can not be applied. Thin film structures are widely used in nano-machines or electronic devices. Therefore, the development of the testing method to evaluate the adhesion strength of thin film and multilayer thin films is needed. Russel et al. [9] have used tape testing and scratch testing methods to measure the interfacial strength of Cu/SiO_2. The tape test is qualitative and often not a reliable test, useful only for testing weakly adhering film. The scratch test is semi-qualitative, in that the normal load at which a predefined failure event or morphology occurs is defined as a measure of adhesion. While these semi-qualitative tests are simple and informative, they are incapable of incorporating all the relevant parameters.

One such quantitative test that retains the same ease of preparation and test conduction as the scratch test is the indentation-induced delamination test. Marshall and Evans and Marshall et al. [10,11] have presented the fracture mechanics analysis of indentation-induced delamination of thin films. Evans and Hutchinson [12] have analyzed the mechanics of the delamination and spalling of compressed films or coatings by using a combination of fracture mechanics and post-buckling theory. Rosenfield et al. [13] have also conducted the indentation-induced delamination tests. They have compared the indentation tests with double-cantilever-beam technique, four-point flexure-beam technique and finite element analyses. Bahr et al. [14] have conducted nano-scale indentation-induced delamination tests. They have used an acoustic emission in conjunction with nanoindentation tests to monitor a delamination or cracking event. Indentation methods generally rely on the formation of a dilated plastic zone in the film to cause the film to blister [15]. Values of G_c, which is fracture toughness of the interface, are related to the indentation volume (or plastic zone size) and extent of debonding. Therefore, this test method suffers from a limitation similar to that the tape test in that it is limited to a very weakly adhered film. In well-adhered films, indentation fails to produce a delamination unless in ordinarily, high loads or depths are used, in which case the substrate deformation renders deconvolution of the adhesion energy from test parameters impossible. However, a modification of this test method has been developed by Kriese et al. [16,17], Gerberich et al. [18] in which the use of a thin hard coating film on the original film to constrain the plastic deformation and brings about the delamination between the original film and substrate.

Other quantitative method for interfacial strength is the pressurized blister test (Jensen [19], Jensen and Thouless [20]). This testing method has been successfully developed and analyzed for thin polymer films, but is often compromised by the inherently compliant loading system, chemical interactions between the debond and the pressurized environment (stress-corrosion cracking), and the etching or machining procedures are needed to produce the cavity.

Some novel testing methods have also proposed. Bagchi et al. [21], Bagchi and Evans [22], Zhuk et al. [23] have developed "superlayer tests," to measure the debond-

ing energy for thin metalization lines on dielectrics. They fabricated Cu films on various dielectric substrates and evaporated superlayers on Cu films to constrain the plastic deformation of Cu layer. Kitamura et al. [24–26] have used a sandwich specimen, where the deformation of thin films is tightly constraint by substrates for preventing the plastic deformation and fracture of thin films and measured the interfacial strength of nanoscale thickness film. Nakasa et al. [27], Zhang et al. [28] have developed the edge-indentation method to measure the delamination strength of thermally sprayed coatings.

The most well known and straightforward method to delaminate the film from the substrate is the peel test. Peel test is a simple mechanical test to measure the adhesion strength, especially for the case of a thin film deposited on a substrate. Many experimental efforts and analyses have been devoted and a comprehensive survey on the earlier development of the subject can be found elsewhere, see Kim and Aravas [29]. For purely elastic case, all earlier works [30–40] identified the following relation among the adhesion strength Γ, the peeling force P and the peeling angle ϕ formed between the interface and the peeling force:

$$\Gamma = P(1 - \cos\phi), \tag{16.1}$$

where P is the forces per unit width of film. When evaluated according to (16.1), the symbol Γ contained a contribution from the residual stress. Moreover, the possible dependence of the adhesion strength on the peeling angle ϕ was not clear at that time. Extensive works [41–47] were devoted to the plastic deformation of the peel as it detached from the substrate, and bend through the moment-curvature hysteresis loop (including plastic loading, elastic unloading, plastic reverse loading, and elastic reverse unloading). A cohesive strip along the leading portion of the interface gives a new twist to the problem. The work by Wei and Hutchinson [48,49] emphasized the influence of cohesive strength improving the nearby plastic dissipation in film and substrate. Their cohesive law [50], however, is normalized in such a way that only an isotropic response with respect to decohesion direction can be accommodated. Other interface cohesive laws (e.g., [51–53]) elaborated several delicate issues of interface debonding. The anisotropic cohesive law by Ma and Kishimoto [51] has the potential to predict a concave adhesive strength versus phase angle curve.

For the interfacial strength of materials used in micro- and opto-electronic devices, Park et al. [54–56] measured the interfacial fracture energy of Cu/Cr/polyimide system by 90° peel test. However, they conducted only one peel angle and it is not enough to discuss the interfacial strength, which is depend on the phase angle. A method of multi-stage peel test (MPT) is proposed in this paper to tackle the issue of measuring adhesion strength as a curve of phase angles. A testing fixture is presented that allows the application of different lateral loads. Balance between the lateral loading and that projected by the peeling load gives rise to a specific peeling angle. Different peeling angles may result for a single film-substrate specimen if one deliberately varies the lateral loads. A steady state peeling load can be achieved after certain amount of decohesion under a prescribed lateral load. MPT involves the measurements on steady state peeling loads for an incremental sequence of lateral loads. These steady state peeling loads are used to correlate the adhesion strength versus phase angle curve.

The plan of this paper is outlined as follows. Testing scheme for MPT will be described in the next section. In Section 16.3, peel tests for copper/chromium/polyimide/silicon substrate will be presented. Those structures are widely used in chip scale packages

(CSP). We will discuss the effect of copper thickness on the interfacial strength and the multi-layer delamination will be considered. The interfacial strength between the conductive thin ceramic film and polymer substrate will be presented in Section 16.4. Those polymer-based films are damaged by ultraviolet rays. We will discuss the degradation of mechanical properties of polymer film and interfacial strength between ceramics and polymer substrates. We also carried out the *in situ* observation of surface cracks on the ceramic layer during the tensile test. The interfacial strength affects the crack formation on the ceramic layer. The concluding remarks with the limitation of multi-stage peel test and future studies will be shown in Section 16.5.

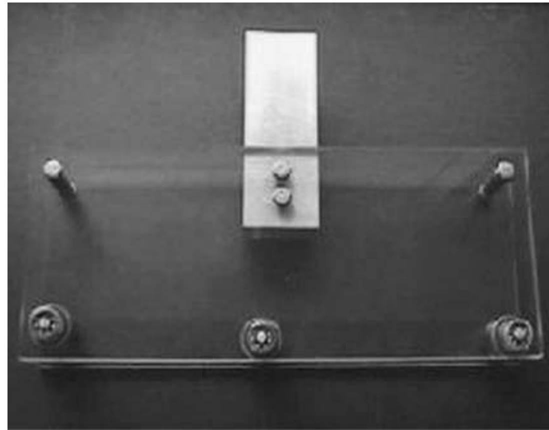

(a)

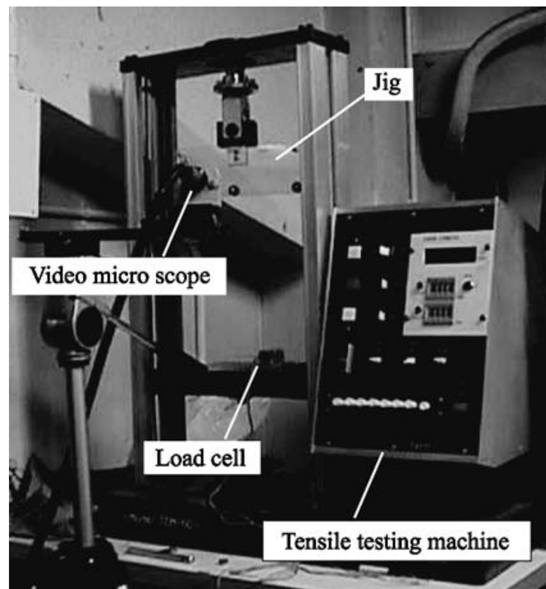

(b)

FIGURE 16.1. The apparatus of multi-stage peel test. (a) Special jig for multi-stage peel test. (b) Setup of the testing machine.

16.2. MULTI-STAGE PEEL TEST (MPT)

Peel tests have been developed for the evaluation of interfacial strength in practical usage, for example, adhesive strength of thin films, coating films. Many papers related to the peel test have also been published (e.g., [29,46]). The most attractive feature of multi-stage peel test is that it is possible to evaluate the interfacial strength of thin films under various phase angles for only one specimen.

16.2.1. Testing Setup

A specially designed apparatus shown in Figure 16.1(a) facilitates the MPT. The special jig is attached to the upper cross head [Figure 16.1(b)] that moves upward at a controlled peeling rate. The movement is recorded by an extensometer. The peeled film is calmed to the lower cross-head that is immobile during a test. A load cell is installed adjacent to the peeling end that records the history of peeling force P. The schematic representation of the MPT is drawn in Figure 16.2. The specimen is put on two roller bearings and by pulling the film, the film delaminates from the substrate. A film/substrate assembly can move horizontally on the bearings with suppressed friction. The friction between rollers and specimen is controlled within less than 0.1 N. During the MPT, the peel front keeps staying near the central bearing and it makes it possible to measure the peel angle continuously. The peel angle was measured and recorded by using the video-microscope and digital video recorder.

As a departure from the conventional peel test, the film/substrate assembly is stretched horizontally by a dead weight P_h through a pulley system that is controlled during the test (in Figure 16.3). Under quasi-static peeling, balance of forces in the horizontal direction predicts the following peel angle:

$$\phi = \cos^{-1}\left(\frac{P_h}{P}\right). \tag{16.2}$$

Vertical component of the peel force is countered by roller supports. To conduct peeling, the force P should be larger that the horizontal stretching force, P_h. The peel angle

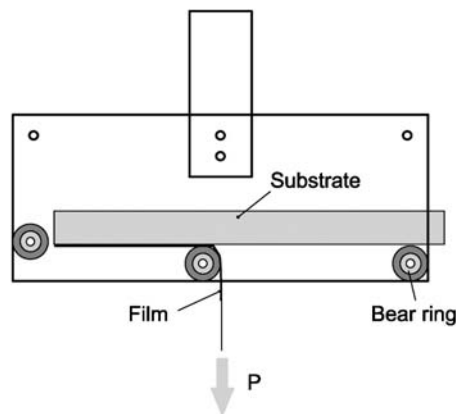

FIGURE 16.2. The schematic representation of peel test.

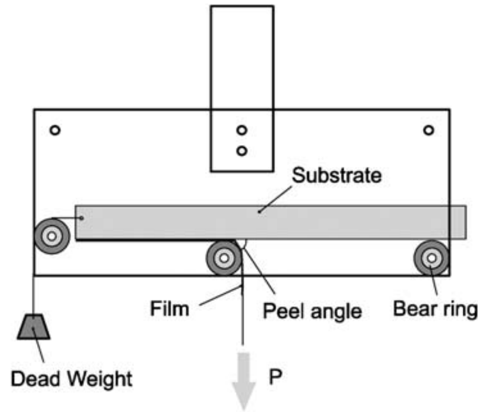

FIGURE 16.3. The dead weight attached on the specimen for changing the peel angle.

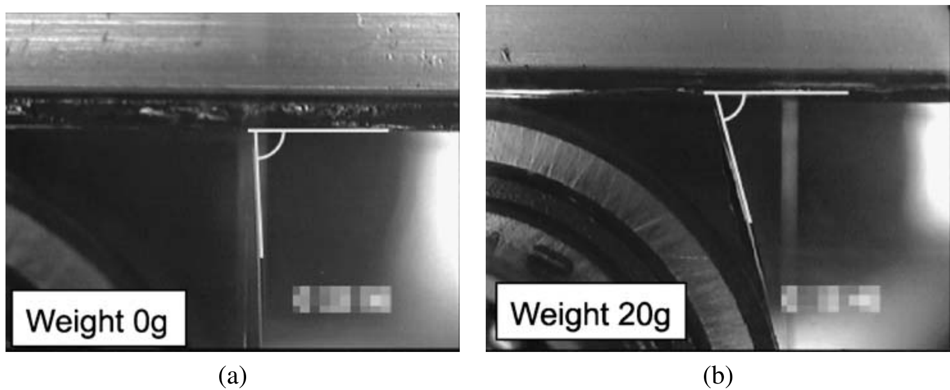

FIGURE 16.4. The effect of the dead weight on the peel angle. (a) No weight. The peel angle is 89°. (b) The dead weight is 20 g. The peel angle is 75°.

decreases monotonically with the increase of P_h. By varying P_h, a wide range of peel angles (between 30 degrees under a large horizontal force to almost 90 degrees for negligible horizontal force) can be achieved. The peel angle can be measured independently and *in situ* by a microscope horizontally mounted on the side facing the test machine, see Figure 16.1(b). A typical image is shown in Figure 16.4. When the dead weight is attached to the specimen, the peel angle changed due to the horizontal force. The relationship between the horizontal force and the peel force decide the peel angle. This effect causes the phase angle shift at the peel front. Therefore, the mixed mode delamination tests under the wide range can be possible by the MPT.

16.2.2. Multi-Stage Peel Test

Figure 16.5 describes a typical curve for the evolution of peel force when the peeling rate maintains at 5 mm/min. A steady state emerges after about 5 mm of peeling length. Samples peeled at other rates (from 1 mm to 5 mm/min) deliver similar results of steady state peeling convened at a peeling length about 5 mm. If the dead load (that controls

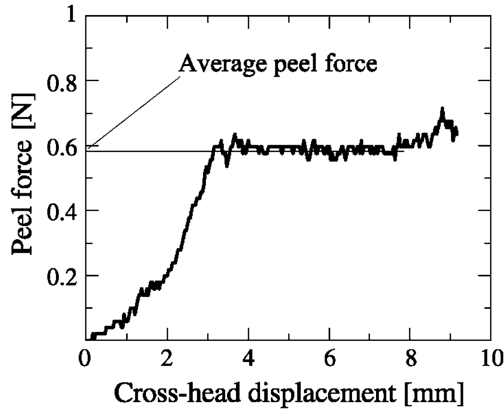

FIGURE 16.5. Typical example of peel force evolution during the MPT.

the horizontal stretching force) is applied incrementally, and a minimum peeling length of 5 mm is imposed on each peeling increment, one can have a multi-stage peeling test in one pass that records the steady state peeling forces at different peeling angles. The apparatus has a lateral span of 220 mm, and the range available for peeling is about 80 mm. Accordingly, over 10 peeling stages can be accommodated in one testing block. Those steady state peeling forces will correlate to the phase angle dependence of adhesion strength in the next section.

16.2.3. Energy Variation in Steady State Peeling

After the attainment of a steady state, the peeling configuration stabilizes. The load point displacement can be chosen as the time variable. Possible rate dependences of the film and the adherent become implicit. Analysis for steady state peeling is further simplified by considering the energetic aspect of the system, as schematically shown in Figure 16.6. During each peeling increment of Δl in a steady state, neither the peeling configuration nor the energy storage and dissipation change for most portion of the system for an observer fixed spatially, say, to the central roller. The only difference in energy exchange consists of a segment of length Δl far behind the peeling edge converting to a segment of the same length far ahead of the peeling edge. The corresponding change in the substrate is negligible since the substrate parts of both segments are essentially stress-free.

Stored in the film far behind the peeling edge is the elastic energy caused by the residual stresses generated during film deposition, the density W_{res} of this energy can be computed as:

$$W_{res} = \frac{\alpha(\nu)}{E} \int_0^h \sigma_{res}^2(y) dy, \tag{16.3}$$

where E and ν denote the Young's modulus and the Poisson's ratio of the film, and σ_{res} denotes the horizontal residual stress stored in the film during deposition. If σ_{res} is uniform across the film thickness h, then

$$W_{res} = \frac{\alpha(\nu)}{E} \sigma_{res}^2 h. \tag{16.4}$$

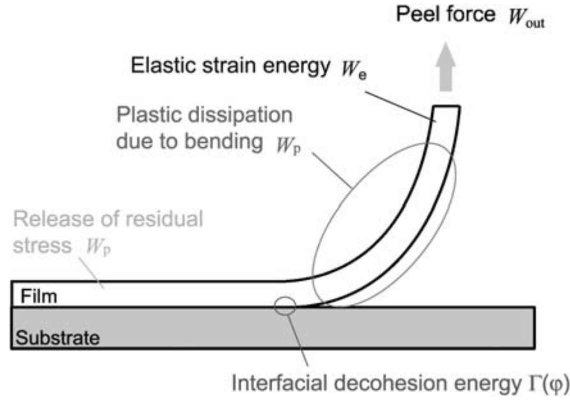

FIGURE 16.6. Energy balance under steady state peeling.

The coefficient $\alpha(\nu)$ depends on the stress state in the film and the Poisson's ratio. It equals to $(1-\nu^2)/2$ for a plane strain film, i.e., see Yu et al. [57] and equals to $1-\nu$ for an equal biaxial stress state caused by thermal mismatch, see Yang and Freund [58].

Near the film end far away from the debonding edge, the energy density comes from the following sources: (1) the decohesion energy, $\Gamma(\varphi)$; (2) the plastic dissipation, W_p, of a certain film moment-curvature hysteresis terminated at the film state near the pulling end; (3) the strain energy due to the residual stress in the film; and (4) the elastic strain energy W_e of the film near the pulling end. For a plane strain situation, the last contribution includes a stretching part of $[(1-\nu^2)/(2Eh)]P^2$ and a coiling part of

$$\frac{Eh^3}{24(1-\nu^2)K_{coil}^2},$$

where K_{coil} is the coiling curvature at the end of the film when it is released from the peeling grip. Contribution from the elastic strain energy W_e is usually small when compared with the others.

Beside the variation of the energies stored or dissipated in the system, the work of the peel force P and that of the dead weight P_h contribute to the potential energy of the system. The rate of those works is denoted as W_{out}, and is given by:

$$W_{out} = P - P_h, \tag{16.5}$$

where, θ is the peel angle measured in the MPT. Apart from the steady state assumption, Equation (16.5) is derived under the ignorance on the work done by all frictional forces. The absence of friction also leads to the equivalence between the raising rate of the dead load and the pulling rate of the lower cross-head when a steady state prevails. Conservation of the potential energy gives:

$$W_{out} = \Gamma(\varphi) + W_p + W_e + W_{res}, \tag{16.6}$$

that is,

$$P - P_h = \Gamma(\varphi) + W_p + \frac{Eh^3}{24(1-\nu^2)K_{coil}^2} + \frac{1-\nu^2}{2E}\left[\frac{P^2}{h} - \int_0^h \sigma_{res}^2(y)dy\right], \tag{16.7}$$

when subjected to a plane strain condition. In Equation (16.7), the material properties such as the Young's modulus E, the Poisson's ratio ν, and those needed in determining W_P can be measured independently. The film thickness h and the dead weight P_h are known *a priori*. The steady state peeling force P and the residual coil curvature K_{coil} can be measured during the test. Appropriate analyses [29,47,48] can be invoked to evaluate W_p. However, one still has the difficulty to distinct the adhesion $\Gamma(\varphi)$ from the contribution of the unknown deposition stress σ_{res} and this value should be measured by another experiments.

The difficulty to obtain the interfacial strength from the above equation is how to estimate the plastic dissipation in detached film. Kim and co-workers [29,46] have proposed a generalized elastic-plastic slender beam theory for the analysis of the detached part of the film in a peel test. They have taken account of elastic unloading and reverse plastic bending of the film and given a closed form solution for the maximum curvature (root curvature) and hence the plastic dissipation, attained by an elastic-perfectly plastic film. Kinloch et al. [47] have studied the peeling of bilinear work hardening materials and found a good agreement with experiment. Since copper thin films are well approximated by bilinear work hardening constitutive equation, we followed the Kinloch et al. [47] approach to estimate the plastic dissipation.

The stress–strain curve at a point on the film cross-section and the moment-curvature diagram are shown in Figures 16.7 and 16.8, respectively. When the loading and unloading of the peeling film both involve plastic deformation, the plastic dissipation energy is correspond to the total energy loss in the loading and unloading cycle, the area [OABC] in Figure 16.8. The plastic dissipation W_p is,

$$W_p = \frac{\Delta \mathrm{OABC}}{b}. \tag{16.8}$$

Thus,

$$W_p = G^e_{\max} f_1(k_0), \tag{16.9}$$

$$W_{out} = G^e_{\max} \frac{1-\cos\theta}{1-\cos(\theta-\theta_0)} f_2(k_0), \tag{16.10}$$

where,

$$\begin{aligned} f_1(k_0) = {} & \frac{4}{3}\alpha(1-\alpha)^2 k_0^2 + 2(1-\alpha)^2(1-2\alpha)k_0 \\ & + \frac{2(1-\alpha)}{3(1-2\alpha)k_0}\left[1+4(1-\alpha)^3\right] - (1-\alpha)\left[1+4(1-\alpha)^2\right], \end{aligned} \tag{16.11}$$

$$\begin{aligned} f_2(k_0) = {} & \frac{1}{3}\alpha\left[1+4(1-\alpha)^2\right] + 2(1-\alpha)^2(1-2\alpha)k_0 \\ & + \frac{8}{3}\frac{(1-\alpha)^4}{(1-2\alpha)k_0} - 4(1-\alpha)^3. \end{aligned} \tag{16.12}$$

$G^e_{\max}$ is the maximum stored elastic energy as defined by,

$$G^e_{\max} = \frac{1}{2} E \varepsilon_y^2 h, \tag{16.13}$$

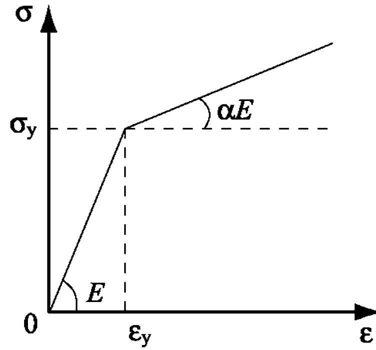

FIGURE 16.7. The stress–strain curve for bilinear, work-hardening material.

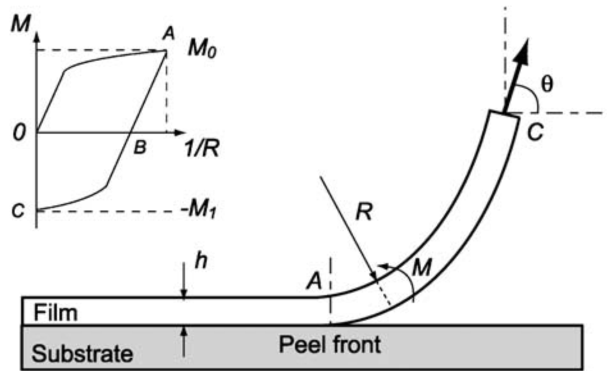

FIGURE 16.8. Deformation of the peeling film and the moment-curvature diagram undergone by peeling film.

and α is the strain hardening coefficient and ε_y is the yield strain. The term k_0 is given by,

$$k_0 = \frac{R_1}{R_0}, \tag{16.14}$$

where R_0 is the actual radius of curvature at the peel front and R_1 is the radius of curvature at the onset of plastic yielding and is given by,

$$R_1 = \frac{h}{2\varepsilon_y}. \tag{16.15}$$

It is noted that the actual radius of curvature at the peel front is difficult to determine, but it is an important parameter. The attached part of the film has been modeled as an elastic beam on an elastic foundation of thickness $h/2$. Applying a beam theory, the relationship of the root angle and k_0 has been obtained as,

$$\theta_0 = \frac{1}{3}(4\varepsilon_y)k_0. \tag{16.16}$$

From Equations (16.10) and (16.16), the root angle and k_0 can be obtained. Then, the plastic dissipation can be calculated from Equation (16.8). The detail of derivation of those equations can be seen in Kinloch et al. [47].

16.3. INTERFACIAL ADHESION STRENGTH OF COPPER THIN FILM

16.3.1. Preparation of Specimen

The specimen used in this paper is composed of copper, chromium, polyimide layers deposited on silicon substrate which is fabricated by the standard method of CSP packages. The cross-sectional view of the specimen is shown in Figure 16.9. The thickness of silicon wafer is about 1 mm, polyimide layer which is coated on Si substrate by spin-coating method is 11 μm and chromium layer which is spattered on polyimide layer is 0.2 μm. The copper layers those are plated on chromium layer are changed as 5, 10 and 20 μm to investigate the effect of copper film thickness on the interfacial strength. The copper spattering layers at the edge of specimen are installed as the scarified layer for the crack initiation. On the multi-stage peel test, the specimen is attached on an aluminum bar (which cross-section is 10 mm × 10 mm) with an epoxy adhesive to prevent the bending of silicon wafer during the peel test.

During the manufacturing process, the residual stresses would be induced in the specimen. Therefore, before peel tests, the residual stresses in copper films were measured by X-ray analysis. The measured residual stresses are shown in Figure 16.10. From this figure, the residual stresses in copper films are less than 3 MPa. The stress relaxation would be occurred in polyimide layer and reduce the residual stresses in copper film. When the residual stresses are assumed to be constant over the film thickness, the dissipation energy needed to release the residual stress can be calculated from Equation (16.4) as shown in Figure 16.10. The dissipation energy is so small that one can neglect the effect of residual stresses in this case.

The stress–strain curve of copper film is necessary to estimate the plastic dissipation as described in previous section. The tensile tests of copper film which thickness is 15 μm were carried out and obtained Young's modulus and 0.2% yield stress. The properties of each material are shown in Table 16.1. Poisson's ratio of copper film and other properties are referred from those of bulk materials.

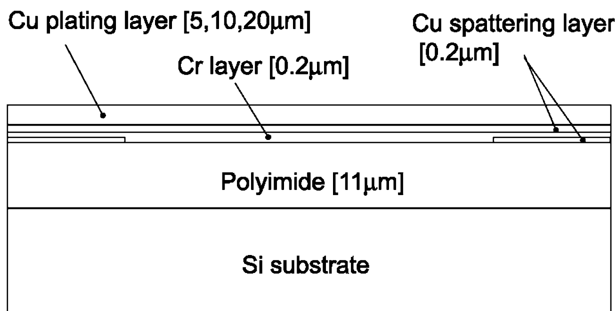

FIGURE 16.9. The cross-sectional view of the specimen.

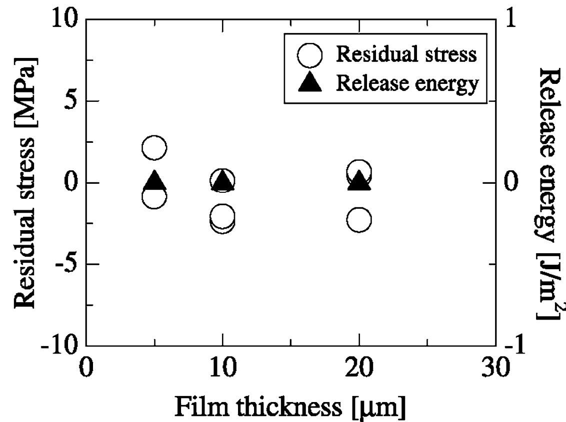

FIGURE 16.10. The residual stresses and the dissipation energy needed to release the residual stresses.

TABLE 16.1.
Material properties of the specimen.

Material	Young's modulus (GPa)	Poisson's ratio	Yield stress $\sigma_{0.2}$ (MPa)
Copper	30	0.3	440
Chromium	115	0.3	—
Polyimide	3	0.45	—

16.3.2. Measurement of Adhesion Strength by the MPT

The characteristic load–displacement curve obtained by the multi-stage peel test is shown in Figure 16.11. After the onset of the peeling, the peel force becomes constant and the delamination is in steady-state condition. Even in steady-state condition, the peel force slightly scatters since the adhesion strength is not locally constant. Hence, we averaged the peel force on some time period for the calculation of the decohesion energy. Figure 16.12 shows the top view of the specimen after the peel test. From the observation of the peeled specimen, the delamination mostly occurred at copper/chromium interface. Therefore, we discuss the interfacial strength of the copper/chromium interface in this paper.

From the averaged peel force and the peel angle, the work done by peel force can be calculated by Equation (16.5). Figure 16.13 shows the work done by peel force, i.e., the energy from outside into the peel front, in no dead weight case. As the film is thinner, the work needed to delaminate becomes larger. From the energy balance of Equation (16.6) and considering the dissipations due to the plastic deformation and the residual stresses, the decohesion energy can be calculated as shown in Figure 16.13. Comparing to the results of the work done by peel force, the effect of film thickness becomes small. When the film thickness is over 10 μm, the decohesion energy becomes constant and is approximately 20 J/m^2. This value is considered to be the interfacial strength between copper and chromium layers. By changing the dead weight attached on the specimen, the dependence of the decohesion energy on the peel angle was obtained in 10, 20 μm cases as shown in Figure 16.14. The peel angles varied from about 45 degrees to 90 degrees and the decohesion energy increase with the peel angles.

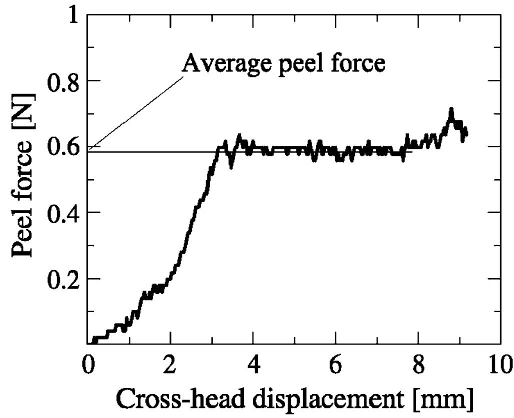

FIGURE 16.11. The characteristic peel force and displacement curve.

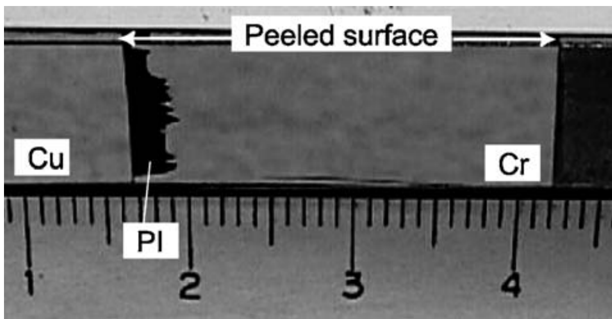

FIGURE 16.12. The top view of the specimen after the peel test. The thickness of Cu layer is 20 μm.

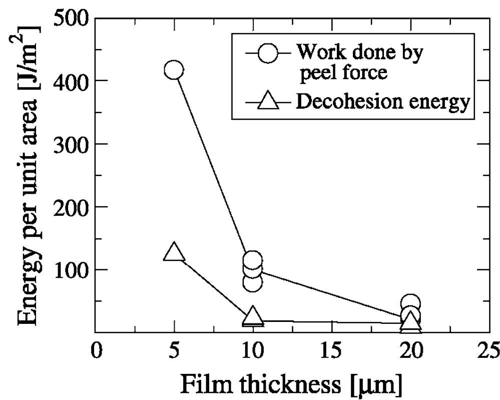

FIGURE 16.13. The work done by peel force and the decohesion energy of Cu/Cr layer.

16.3.3. Discussions

In previous section, we obtained the decohesion energy of copper and chromium interface by the multi-stage peel test. However, it should be considered whether this obtained

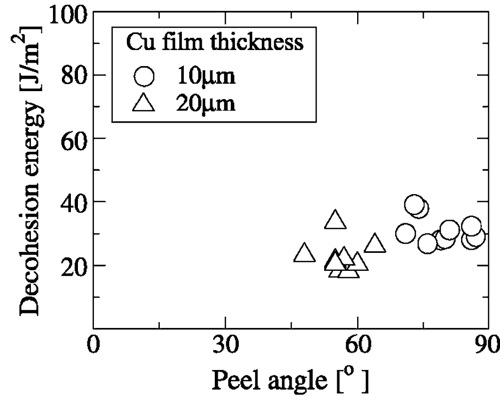

FIGURE 16.14. The peel angle effects on the decohesion energy.

value is reasonable or not. To confirm it, we have carried out finite element analysis and compare experimental results with numerical results. During the steady-state condition, the peel problem can be divided to the detached part and attached part as shown in Figure 16.15. Our interest is the energy flow around the peel front. Then, we can only consider the attached part with appropriate boundary conditions. From the equilibrium condition of force and moment between detached and attached part, the boundary conditions can be obtained as:

$$\left.\begin{array}{l} N = F\cos\theta - F_h \\ Q = F\sin\theta \\ M = F\sin\theta \cdot d \end{array}\right\}, \tag{16.17}$$

where, F is the averaged peel force, F_h is the dead weight, θ is the peel angle and d is the reference length from the peel front at which the peel angle is measured. Then, the numerical model of the multi-stage peel test is reduced to the equivalent interface crack problem as shown in Figure 16.16. In this case, silicon substrate is assumed to be rigid for simplicity.

From experiments, the averaged peel forces and peel angles during the steady-state condition were measured. Those values are used as the boundary conditions for numerical simulations. The interfacial fracture energy, which is correspond to the decohesion energy, was evaluated by J-integral in numerical simulations. Figure 16.17 shows the comparison between the results of the MPT method and J-integral calculation. In elastic analyses, the results of the J-integral calculation agree well with the MPT results, but the obtained results depend on film thickness. On the other hand, in elastic-plastic analyses, the J-integral values become constant, about 20 J/m^2, and are independent of film thickness. J-integral value for elastic-plastic material still has the meaning of energy release rate. Hence, this value is considered to be the interfacial strength of Cu/Cr interface. The difference between the MPT results and J-integral values stems from the formation of plastic zone around the peel front. Not only bending of the film but also stress concentration at the peel front induced the plastic deformation at the peel front. The plastic zone ahead of peel front is shown in Figure 16.18. In 20 μm case, the plastic zone is formed at the vicinity of the peel front and can be neglected like the small-scale yielding condition. On the contrary, in 5 μm case, the copper film is largely bended and the plastic zone is formed around the peel front

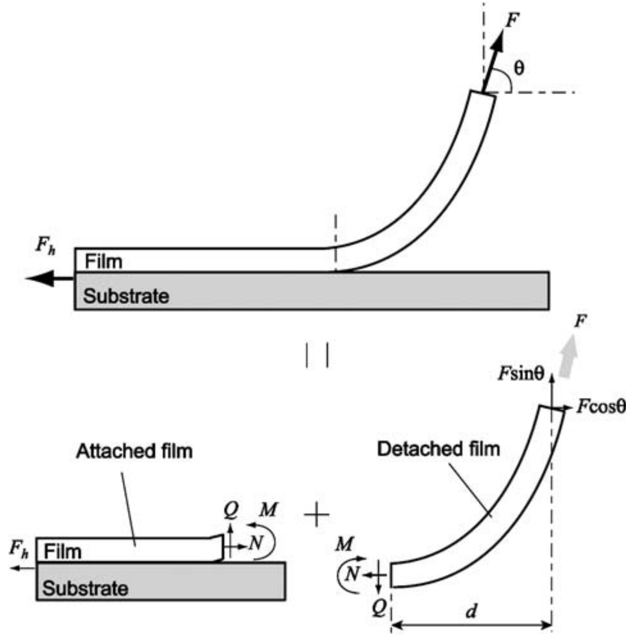

FIGURE 16.15. The reduction of solved problem into the equivalent interface crack problem.

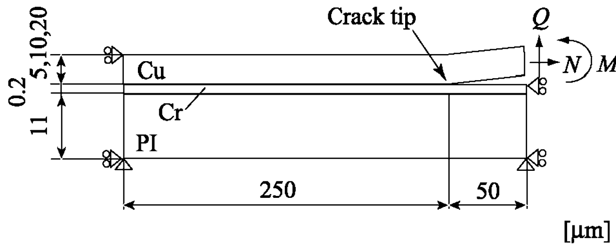

FIGURE 16.16. Numerical model for multi-stage peel test.

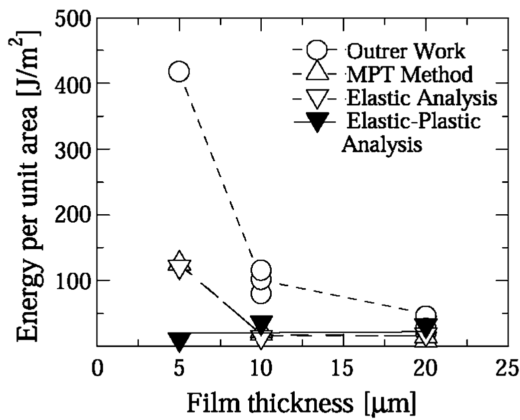

FIGURE 16.17. Comparison with the results of MPT and numerical simulation.

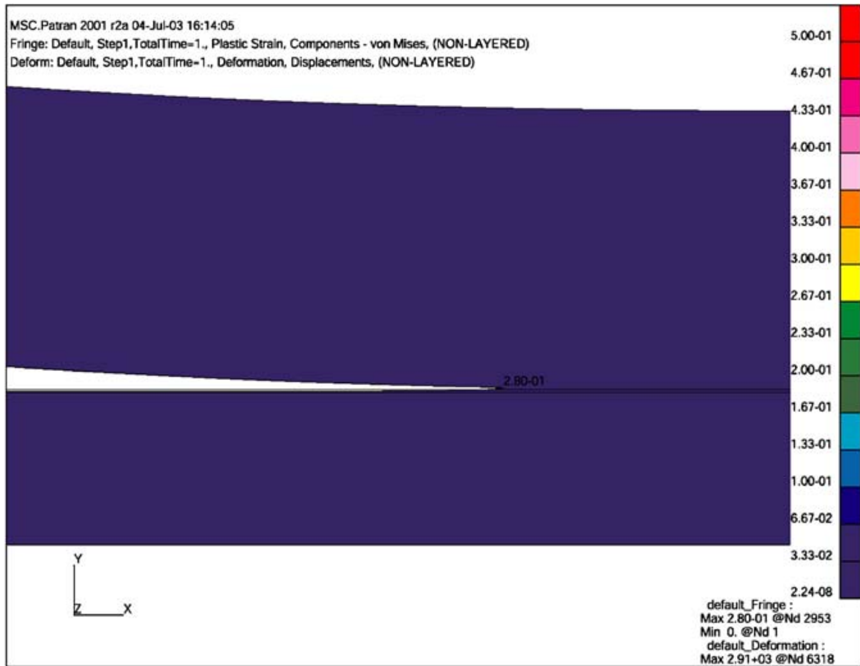

(a)

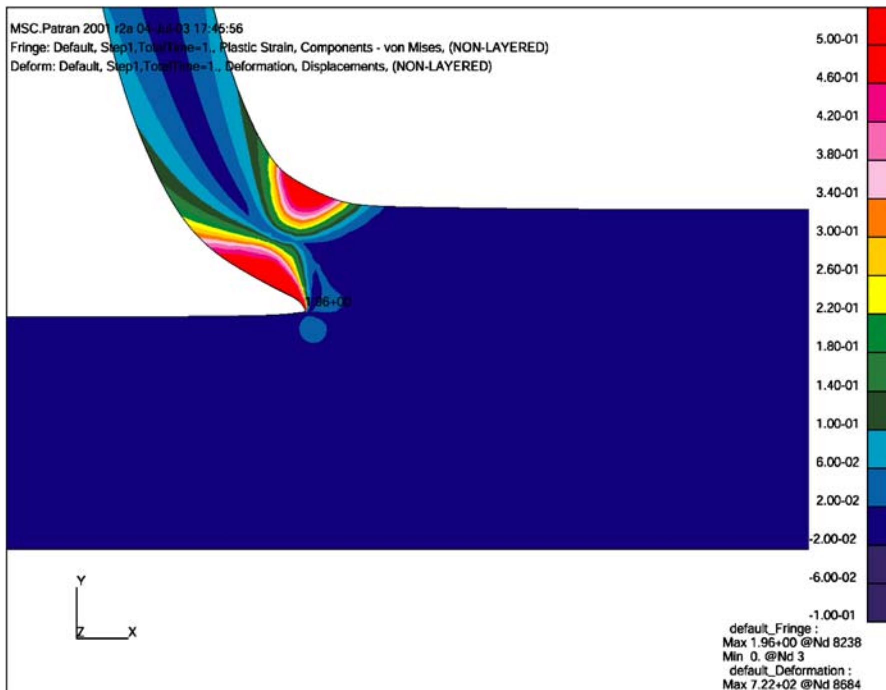

(b)

FIGURE 16.18. The plastic strain distribution around the peel front. (a) Copper film thickness is 20 μm. (b) Copper film thickness is 5 μm.

widely. This case is corresponding to the large-scale yielding condition. The energy evaluation in the MPT method does not cover the large-scale yielding condition. Therefore, the MPT evaluation includes the energy dissipation due to the plastic deformation.

The J-integral evaluation in 5 μm case is slightly smaller than the other cases. This means that the decohesion energy between copper and chromium is smaller than the other cases. To consider this difference, the surface observation of peeled specimen was carried out by Atomic Force Microscope (AFM). Figure 16.19 shows the results of surface observation after the multi-stage peel test. The chromium surface is very flat and the roughness is less than a few nano-meter in 20 μm case. On the other hand, in 5 μm case, small hills those heights were about 40 nm were observed. These results imply that the delamination of Cr/PI and Cu/Cr occurred simultaneously during the peel test. Figure 16.20 shows the mean stress distribution on Cr/PI interface and high mean stress concentration occurred ahead of the peel front. This mean stress may expand micro or nano voids on Cr/PI interface and induce the delamination on Cr/PI interface. The decohesion energy measured by the MPT method for 5 μm case includes the decohesion energy both Cu/Cr and Cr/PI interfaces. The delamination occurred between Cr and PI layers may influence the stress distribution and constrain the plastic deformation ahead of the peel front. The finite element analyses did not consider the multiple delamination and it overestimated the plastic dissipation than the realistic case. Hence, the J-integral evaluation in 5 μm case is slightly smaller than the other cases.

The MPT evaluation gives us only the energy flow into the peel front and does not eliminate the energy dissipation around the peel front, such as plastic dissipation. Therefore, the MPT method can be applied to the peeling under small-scale yielding condition. Nowadays, the film thickness becomes thinner and thinner going down to nano or sub-nano thickness in electronic devices. In those situations, the multiple delamination would be one of critical issues. The development of precious evaluation methods for multi-layer systems are needed and left in future works.

16.4. UV-IRRADIATION EFFECT ON CERAMIC/POLYMER INTERFACIAL STRENGTH

It is well known that the mechanical properties of polymers, such as tensile strength or rupture strain, are degraded by the irradiation of ultraviolet (UV) rays. When the polymer-based conductive films are used in the open air, it is necessary to consider the degradation of the mechanical properties in design of products. The bonding mechanism between ceramic and polymer is mainly intermolecular force. When UV rays irradiate polymeric materials, the principal chains are cut and oxidized. Those reactions may affect the bonding strength between ceramics and polymers. That is the motivation of this research and we investigated the effects of UV irradiation on the interfacial adhesion strength between ITO (indium tin oxide) coating layer and PET (poly(ethylene terephthalate)) substrate by multi-stage peel test.

16.4.1. Preparation of PET/ITO Specimen

Two types of specimens were prepared. One type is composed of ITO and PET and the other is composed of ITO, TiO_2 and PET. All specimens were fabricated by spattering ITO or TiO_2 on PET substrate. The thickness of each layer is summarized in Table 16.2.

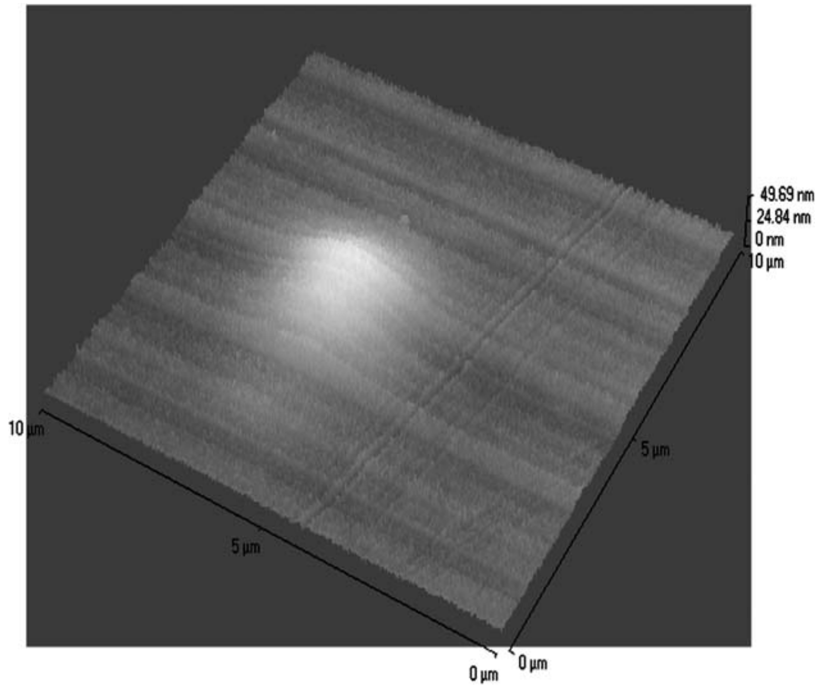

(a)

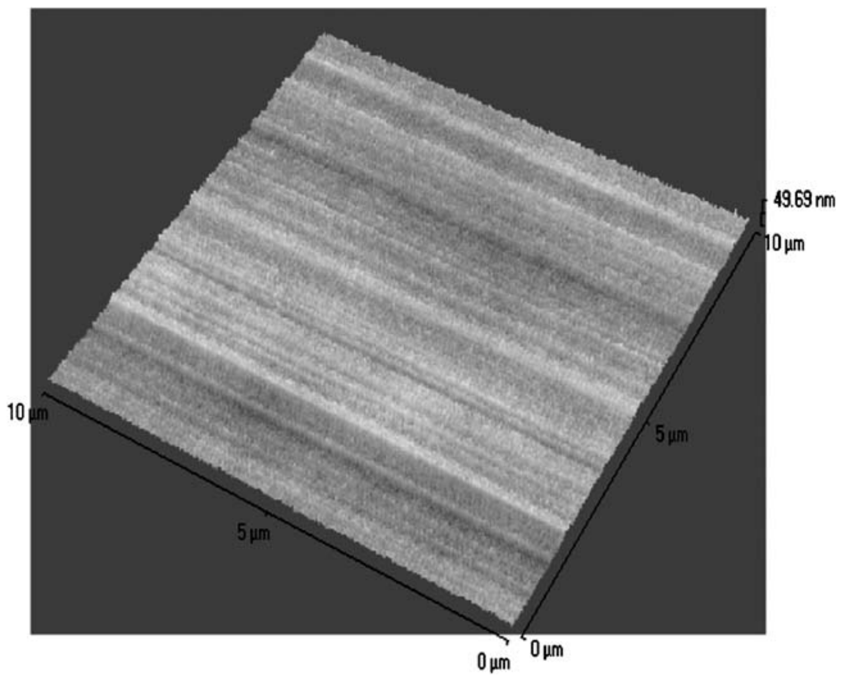

(b)

FIGURE 16.19. The Cr surface configuration after the peel test. (a) The thickness of Cu layer is 5 µm. (b) The thickness of Cu layer is 20 μm.

To investigate the effect of UV irradiation, half of specimens were kept in a fade meter for 120 hours. The UV ray is exposed on ITO face and the intensity of UV ray is about 30 W/m^2. The cross-sectional view of the specimen is shown in Figure 16.21. The specimen was attached on aluminum bar with an epoxy adhesive, since the specimen was too thin to conduct the peel test directly. The stress–strain curves of PET film needed to estimate the plastic dissipation are shown in Figure 16.22. The stress–strain relation depends on the direction of loading. Young's modulus and yield stresses are summarized in Table 16.3. After UV irradiation, the rupture strain gradually decreased. The relation between rapture strain and irradiation period is represented in Figure 16.23. The rupture strain becomes smaller and smaller, as the irradiation time become long. After 120 hour irradiation, PET film is ruptured almost within elastic region.

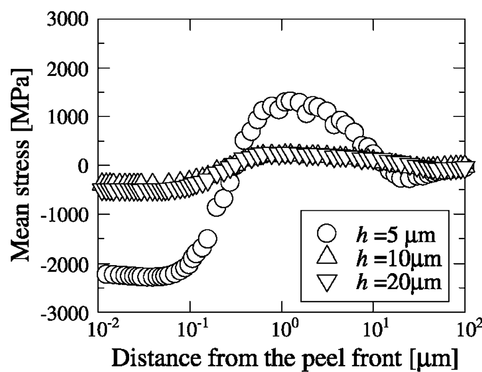

FIGURE 16.20. The mean stress distribution on chromium and polyimide interface.

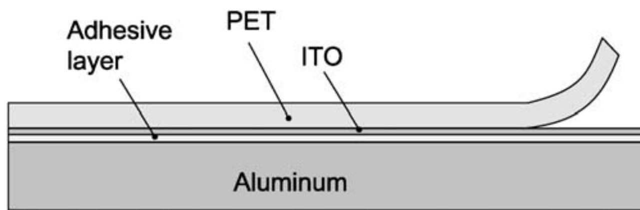

FIGURE 16.21. The cross-sectional view of test specimen.

TABLE 16.2.
The condition of test specimen.

Name	PI	PIUV	PIT	PITUV
Substrate	PET 100 μm	PET 100 μm	PET 100 μm	PET 100 μm
Coating layer	ITO 108 nm	ITO 108 nm	ITO/TiO_2 100/20 nm	ITO/TiO_2 100/20 nm
UV	—	120 hours	—	120 hours

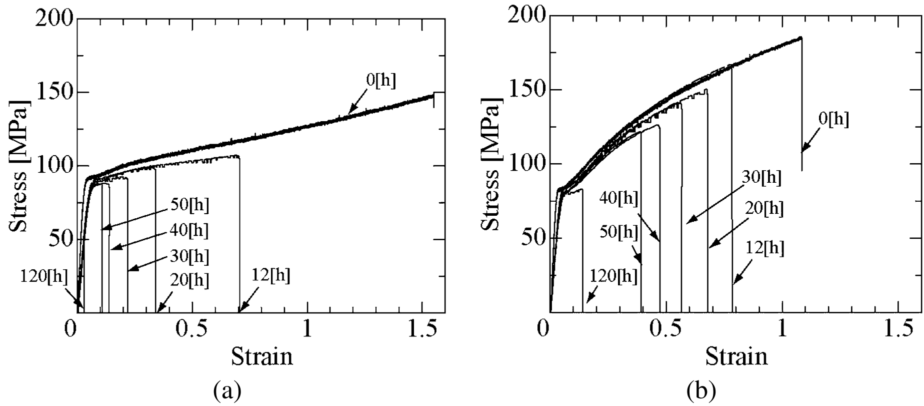

FIGURE 16.22. The stress–strain relation of PET film. (a) Parallel to the rolling direction. (b) Vertical to the rolling direction.

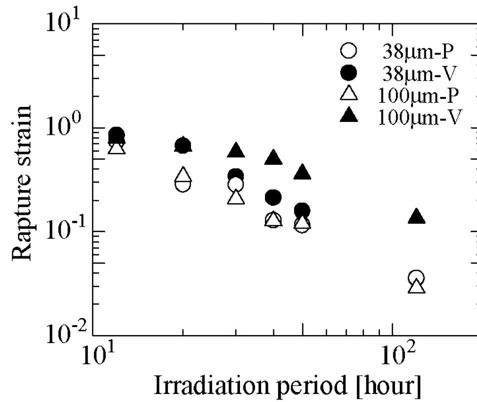

FIGURE 16.23. The irradiation effects on rupture strain of PET film.

TABLE 16.3.
Mechanical properties of PET film.

Name	LT	TL	Name	LT	TL
Young's modulus	3.8 GPa	4.1 GPa	Strain hardening coefficient, α	0.105	0.194
Poisson's ratio	0.41	0.49	Yield strain, ε_y	0.028	0.02

16.4.2. Measurement of Interfacial Strength by MPT

The load history during the peel test for PET/ITO specimen is shown in Figure 16.24. and the peel angle at the peel front during the peel test is shown in Figure 16.25. When the dead weight is about 0.83 N, the peel angle is about 55°. Without the dead weight, the peel angle is about 71°. From the load history (Figure 16.24) and the peel angle at that time, the

work done by peel force can be calculated from Equation (16.5). Also, the plastic dissipation in PET film can be estimated by Equation (16.8). When neglecting the residual stress in PET film because of the relaxation of polymeric material, the decohesion energy, then, can be evaluated from Equation (16.7). The decohesion energy by MPT method is shown in Figure 16.26 and 16.27. Figure 16.26 represents the decohesion energy of PET/ITO interface. For virgin films, the interfacial strength is about 20 J/m^2 and slightly depends on the peel angle. On the other hand, after UV irradiation, the interfacial strength is drastically decreased about 1 to 10 J/m^2 and clearly depends on the peel angle. Figure 16.27 represents the decohesion energy for PET/TiO_2/ITO specimen. The delamination occurred between PET and TiO_2 interface and the decohesion energy correspond to the interfacial strength between PET and TiO_2. In this case, for virgin films, the decohesion energy is smaller than that of PET/ITO interface. However, the degradation of interfacial strength due to UV irradiation is smaller than that of PET/ITO interface. It is considered that TiO_2 layer works as a filter and it makes the intensity of UV ray transmitted to PET layer smaller. Therefore, inserting TiO_2 layer between ITO and PET is useful to prevent the degradation of interfacial strength.

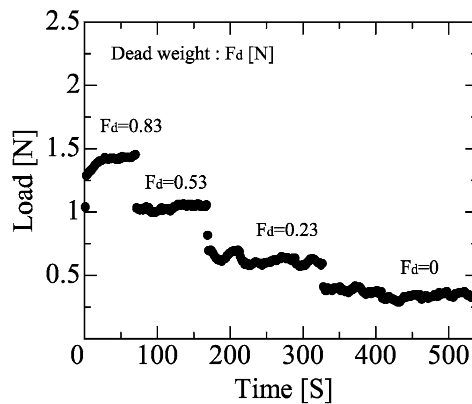

FIGURE 16.24. Load history of multi-stage peel test (PET/ITO_{LT}).

FIGURE 16.25. Measurement of peel angle: (a) dead weight is 0.83 N, (b) no dead weight.

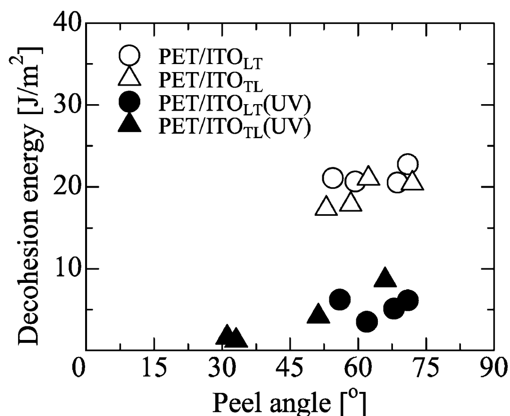

FIGURE 16.26. Decohesion energy of PET/ITO interface and effect of UV irradiation.

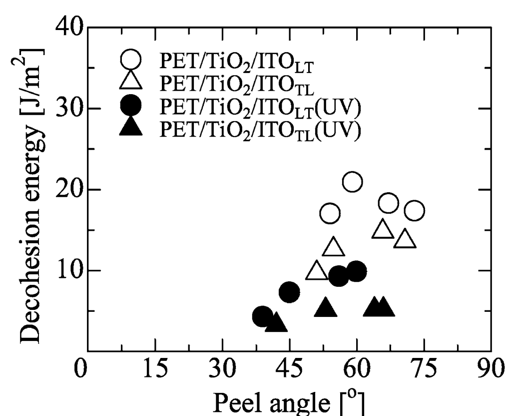

FIGURE 16.27. Decohesion energy of PET/TiO_2 interface and effect of UV irradiation.

16.4.3. Surface Crack Formation on ITO Layer under Tensile Loading

Cracks easily formed on ITO layer under tensile loading since ITO is a brittle ceramic. Once the surface crack is formed, the functionality of the complex film will be lost. Our interest is how the interfacial strength affects the crack formation on ITO layer. Therefore, in this sub-section, we carried out the tensile tests for PET/ITO complex film and the *in situ* observation of the ITO surface.

The small tensile testing machine was used under the confocal laser scanning microscope. The rectangular specimen was prepared which width is 1 mm and length is 50 mm. The stress–strain relation of the complex film is shown in Figure 16.28. It is noted that the strain is measured from the cross head displacement divided by the initial length between cramps. The stress–strain relation is almost same with that of PET film and the mechanical properties of these complex films are decided by that of PET film. However, the rupture strain is larger than that of PET film. This is because ITO layer make the intensity of UV ray reached to PET film weaker.

The *in situ* observation of surface crack formation is shown in Figure 16.29. When the strain reached 2.8%, "vertical cracks" can be observed on ITO layer. The distance between

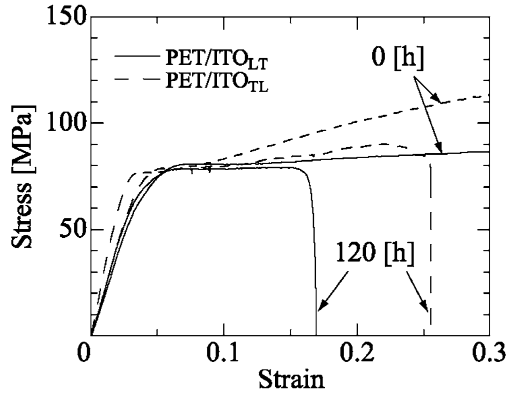

FIGURE 16.28. The stress–strain relation of PET/ITO specimen.

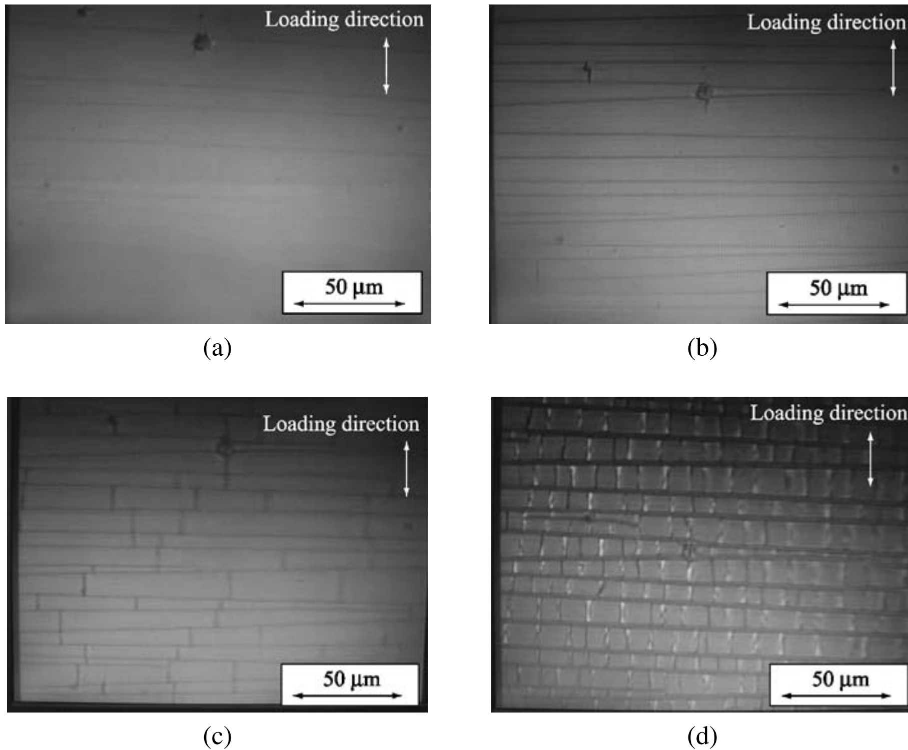

FIGURE 16.29. *In situ* observation of PET/ITO$_{LT}$ surface during tensile test. (a) $\varepsilon = 2.8\%$, (b) $\varepsilon = 6.4\%$, (c) $\varepsilon = 12\%$, (d) $\varepsilon = 30\%$.

cracks is almost constant. The density of cracks increased with applied strain as shown in Figure 16.29(b). The driving force of crack formation is shear force between ITO and PET layers [59,60]. When the interfacial strength is large, the interfacial shear rigidity is stiff and the same strain within PET film will be induced in ITO layer. That brings about high tensile stress in ITO layer and cracks are formed even in small strain range. After the strain reached about 12%, "parallel cracks" to the loading direction were observed. Due

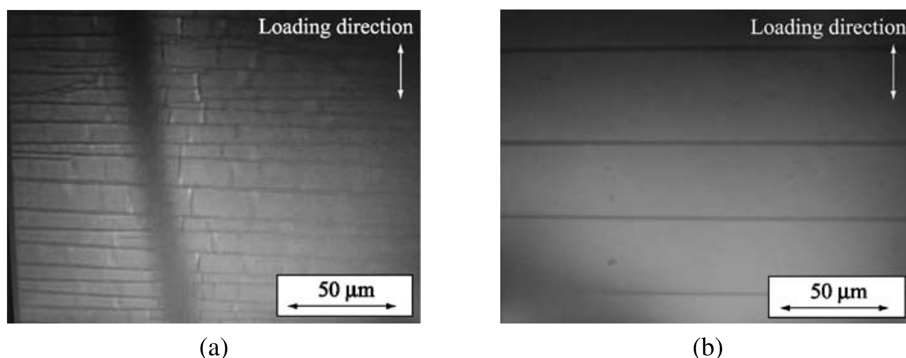

FIGURE 16.30. The effect of UV irradiation on the fracture pattern of PET/ITO_{TL} surface: $\varepsilon = 10\%$. (a) Virgin specimen. (b) UV-irradiated specimen (120 hours).

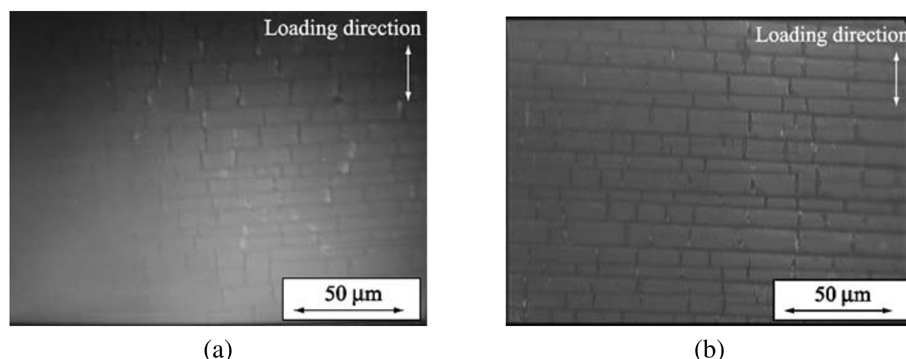

FIGURE 16.31. The effect of UV irradiation on the fracture pattern of PET/TiO_2/ITO_{TL} surface: $\varepsilon = 10\%$. (a) Virgin specimen. (b) UV-irradiated specimen (120 hours).

to the Poisson's effect, the compressed stress vertical to the loading direction induced and buckling cracks occurred in ITO layer. After the initiation of buckling crack, the density of "vertical cracks" is constant and only the density of "parallel cracks" increased.

The comparison of UV irradiation effects on crack formation is shown in Figure 16.30 and 16.31. Figure 16.30 represents of PET/ITO_{TL} specimen at the tensile strain is about 10%. After UV irradiation for 120 hours, only "vertical cracks" can be observed. This is because the interfacial strength between PET and ITO decreased by UV irradiation as shown in Figure 16.26 and then, the interfacial shear rigidity also decreased. Even when PET layer deformed largely, the strain induced in ITO layer can not be enough to form "parallel cracks." On the other hand, the crack formation of PET/TiO_2/ITO specimen is almost same as that of virgin specimen as shown in Figure 16.31. In this case, the degradation of the interfacial strength is smaller than that of PET/ITO case. From these results, the interfacial strength closely related the crack formation behavior on ITO layer.

16.5. CONCLUDING REMARKS

In this chapter, the multi-stage peel test method is introduced and is applied to the measurement of the adhesion strength for copper thin film and conductive ceramics film.

During the steady-state peeling, the interfacial strength can be evaluated by the energy balance of peeling system. When the film thickness is thick enough to neglect the plastic zone size at the peeling tip, i.e., under small-scale yielding condition, MPT method can be valid to evaluate the interfacial strength precisely. However, when the film thickness is thinner and the plastic zone size can not be neglected, i.e., under large-scale yielding condition, the MPT method can not be applied directly and needs the help of some numerical calculations. More, in multi-layer system, the delamination on other layers would be occurred during peel tests. In those cases, the delamination of other layers will affect the stress condition at the peeling tip and the conventional evaluation techniques can not be applied. Those multiple delamination would be important issues in nano- and subnano-thickness film structures and the solution of those problems has been left in future works.

We also applied MPT method to the measuring of the interfacial strength between conductive ceramics thin film (ITO) and polymer substrate (PET). The stress–strain relations of PET film are significantly degraded by UV irradiation. The interfacial strength between ITO and PET was also degraded. When TiO_2 layer inserted between ITO and PET layers, the degradation of interfacial strength became smaller than that of PET/ITO interface. TiO_2 layer works as a filter and protect the interfacial bonding between ITO and PET from UV attack. The interfacial strength is closely related to the crack formation of ITO layer under tensile loadings. However, it has not been clear how much molecules on the interface or under the interface are damaged by UV irradiation and how to connect the number of damaged molecules and the degradation of interfacial strength quantitatively. The bottom-up approaches, such as molecular dynamics, are necessary to solve these problems. Moreover, when supplying the power voltage on ITO layer, the interfacial strength and crack formation would be different from obtained results. Therefore, it is necessary to conduct those experiments under more realistic situations.

ACKNOWLEDGMENT

The authors would like to acknowledge Dr. Amagai of Texas Instruments Japan and Dr. Yanaka of Toppan Printing Co. Ltd., for their preparation of test specimen.

REFERENCES

1. S.F. Al-sarawi, D. Abbott, and P.D. Franzon, A review of 3-D packaging technology, IEEE Transactions on Components, Packaging and Manufacturing Technology, Part B, 21, pp. 2–14 (1998).
2. E. Harlev, T. Gulakhmedova, I. Rubinovich, and G. Aizenshtein, New method for the preparation of conductive polyaniline solutions: Application to liquid crystal devices, Advanced Materials, 8, pp. 994–997 (1996).
3. G. Gu, P.E. Buroows, S. Venkatesh, S.R. Forrest, and M.E. Thompson, Vacuum-deposited, nonpolymeric f lexible organic light-emitting devices, Optics Letters, 22, pp. 172–174 (1997).
4. Z. Chen, B. Cotterell, W. Wang, E. Guenther, and S.J. Chua, A mechanical assessment of flexible optoelectronic devices, Thin Solid Films, 394, pp. 201–205 (2001).
5. M. Notomi, T. Gotoh, K. Kishimoto, and T. Shibuya, Evaluation of ultra-violet degradation on PP and PC by layering-films exposure test, Transactions of the Japan Society of Mechanical Engineers, Part A, 63, pp. 437–444 (1997).
6. J.W. Hutchinson and Z. Suo, Mixed mode cracking in layered materials, Advances in Applied Mechanics, 29, pp. 63–191 (1992).
7. A.G. Evans and J.W. Hutchinson, The thermomechanical integrity of thin films and multilayers, Acta Metallurgica Materialia, 43, pp. 2507–2530 (1995).

8. A.G. Evans, J.W. Hutchinson, and Y. Wei, Interface adhesion: effects of plasticity and segragation, Acta Metallurgica Materialia, 47, pp. 4093–4113 (1999).
9. S.W. Russel, S.A. Rafalski, R.L. Spreitzer, J. Li, M. Moinpour, F. Moghadam, and T.L. Alford, Enhanced adhesion of copper to dielectrics via titanium and chromium additions and sacrificial reactions, Thin Solid Films, 262, pp. 154–167 (1995).
10. D.B. Marshall and A.G. Evans, Measurement of adherence of residually stressed thin films by indentation. I. Mechanics of interfaced delamination, Journal of Applied Physics, 56, pp. 2632–2638 (1984).
11. C. Rossington, A.G. Evans, D.B. Marshall, and B.T. Khuri-Yakub, Measurement of adherence of residually stressed thin films by indentaion. II. Experiments with ZnO/Si, Journal of Applied Physics, 56, pp. 2639–2644 (1984).
12. A.G. Evans and J.W. Hutchinson, On the mechanics of delamination and spalling in compressed films, International Journal of Solids and Structures, 20, pp. 455–466 (1984).
13. L.G. Rosenfeld, J.E. Ritter, T.J. Lardner, and M.R. Lin, Use of the microindentation technique for determining interfacial fracture energy, Journal of Applied Physics, 67, pp. 3291–3298 (1990).
14. D.F. Bahr, J.W. Hoehn, N.R. Moody, and W.W. Gerberich, Adhesion and acoustic emission analysis of failures in nitride films with a metal interlayer, Acta Materialia, 45, pp. 5163–5175 (1997).
15. M.D. Drory and J.W. Hutchinson, Measurement of the adhesion of a brittle film on a ductile substrate by indentation, Proceedings of the Royal Society of London Series A—Mathematical Physical and Engineering Sciences, 452, pp. 2319–2341 (1996).
16. M.D. Kriese, N.R. Moody, and W.W. Gerberich, Effects of annealing and interlayers on the adhesion energy of copper thin films to SiO2/Si substrate, Acta materialia, 46, pp. 6623–6630 (1998).
17. M.D. Kriese, D.A. Boismier, N.R. Moody, and W.W. Gerberich, Nonomechanical fracture-testing of thin films, Engineering Fracture Mechanics, 61, pp. 1–20 (1998).
18. W.W. Gerberich, D.E. Kramer, N.I. Tymiak, A.A. Volinsky, D.F. Bahr, and M.D. Kriese, Nanoindentation-induced defect-interface interactions: phenomena. Methods and limitations, Acta Materialia, 47, pp. 4115–4123 (1999).
19. H.M. Jensen, The blister test for interface toughness measurement, Engineering Fracture Mechanics, 40, pp. 475–486 (1991).
20. H.M. Jensen and M.D. Thouless, Effects of residual stresses in the blister test, International Journal of Solids and Structures, 30, pp. 779–795 (1993).
21. A. Bagchi, G.E. Lucas, Z. Suo, and A.G. Evans, A new procedure for measuring the decohesion energy for thin ductile films on substrates, Journal of Material Research, 9, pp. 1734–1741 (1994).
22. A. Bagchi and A.G. Evans, Measurements of the debond energy for thin metallization lines on dielectrics, Thin Solid Films, 286, pp. 203–212 (1996).
23. A.V. Zhuk, A.G. Evans, J.W. Hutchinson, and G.M. Whitesides, The adhesion energy between polymer thin films and self-assembled monolayers, Journal of Material Research, 13, pp. 3555–3565 (1998).
24. T. Kitamura, T. Shibutani, and T. Ueno, Development of evaluation method for interface strength between thin films and its application on delamination of Cu/TaN in an advanced LSI, Transactions of the Japan Society of Mechanical Engineers, 66, pp. 1568–1573 (2000).
25. T. Kitamura, H. Hirakata, and T. Itsuji, Delamination strength of Cu thin film characterized by nanoscale stress field near interface edge, Transactions of the Japan Society of Mechanical Engineers, Part A, 68, pp. 119–125 (2002).
26. T. Kitamura, H. Hirakata, and Y. Yamamoto, Interface strength of tungsten micro-component on silicon substrate by means of AFM, Transactions of the Japan Society of Mechanical Engineers, Part A, 69, pp. 1216–1221 (2003).
27. K. Nakasa, M. Kato, D. Zhang, and K. Tasaka, Evaluation of delamination strength of thermally sprayed coating by edge-indentation method, Journal of the Society of Material Science, Japan, 47, pp. 413–419 (1998).
28. D. Zhang, M. Kato, and K. Nakasa, Fracture mechanics analysis of edge-indentation method for evaluation of delamination strength of coating, Journal of the Society of Material Science, Japan, 49, pp. 572–578 (2000).
29. K.S. Kim and N. Aravas, Elasto-plastic analysis of the peel test, International Journal of Solids and Structures, 24, pp. 417–435 (1988).
30. G.J. Spies, The peeling test on redux-bonded joints, Journal of Aircraft Engineering, 25, pp. 64–70 (1953).
31. J.J. Bickerman, Theory of peeling through a hookean solid, Journal of Applied Physics, 28, pp. 1484–1485 (1957).
32. D.H. Kaeble, Theory and analysis of peel adhesions: mechanism and mechanics, Transaction of Society of Rheology, 3, pp. 161–180 (1959).

33. D.H. Kaeble, Theory and analysis of peel adhesions: bond stresses and distributions, Transaction of Society of Rheology, 4, pp. 45–73 (1960).
34. C. Jouwersma, On the theory of peeling, Journal of Polymer Sciences, 45, pp. 253–255 (1960).
35. S. Yurenka, Peel testing of adhesive bonded metal, Journal of Applied Polymer Science, 6, pp. 136–144 (1962).
36. J.L. Gardon, Peel adhesion. II. A theoretical analysis, Journal of Applied Polymer Sciences, 7, pp. 643–664 (1963).
37. E.B. Saubestre, L.J. Durney, J. Haidu, and E. Bastenbeck, The adhesion of electrodeposits to plastics, Plating, 52, pp. 982–1000 (1965).
38. K. Kendall, The shapes of peeling solid films, Journal of Adhesion, 5, pp. 105–117 (1973).
39. A.N. Gent and G.R. Hamed, Peel mechanics, Journal of Adhesion, 7, pp. 91–95 (1975).
40. D.W. Nicholson, Peel mechanics with large bending, International Journal of Fracture, 13, pp. 279–287 (1977).
41. M.D. Chang, K.L. Devries, and M.L. Williams, The effects of plasticity in adhesive fracture, Journal of Adhesion, 4, pp. 221–231 (1972).
42. A.N. Gent and G.R. Hamed, Peel mechanics for an elastic-plastic adherent, Journal of Applied Polymer Sciences, 21, pp. 2817–2831 (1977).
43. A.D. Crocombe and R.D. Adams, Peel analysis using the finite element method, Journal of Adhesion, 12, pp. 127–139 (1981).
44. A.D. Crocombe and R.D. Adams, An elasto-plastic investigation of the peel test, Journal of Adhesion, 13, pp. 241–267 (1982).
45. A.G. Atkins and Y.W. Mai, Residual strain energy in elastoplastic adhesive and cohesive fracture, International Journal of Fracture, 30, pp. 203–221 (1986).
46. K.-S. Kim and J. Kim, Elasto-plastic analysis of the peel test for thin film adhesion, Journal of Engineering Materials and Technology, 110, pp. 266–273 (1988).
47. A.J. Kinloch, C.C. Lau, and J.G. Williams, The peeling of flexible laminates, International Journal of Fracture, 66, pp. 45–70 (1994).
48. Y. Wei and J.W. Hutchinson, Interface strength, work of adhesion and plasticity in the peel test, International Journal of Fracture, 93, pp. 315–333 (1998).
49. Y. Wei and J.W. Hutchinson, Peel test and interfacial toughness, in W. Gerberich and W. Yang, Eds., Interfacial and Nanoscale Failure, Volume 8, Comprehensive Structural Integrity, I. Milne, R.O. Ritchie, and B. Karihaloo, Editors-in-Chief, Elsevier, Amsterdam, 2003, pp. 181–217.
50. V. Tvergaard and J.W. Hutchins, The influence of plasticity on mixed mode interface toughness, Journal of the Mechanics and Physics of Solids, 41, pp. 1119–1135 (1993).
51. F. Ma and K. Kishimoto, A continuum interface debonding model and application to matrix cracking of composite, JSME International Journal, Series A, 39, pp. 496–507 (1996).
52. C. Zhou, W. Yang, and D. Fang, Damage of short-fiber-reinforced metal matrix composite considering cooling and thermal cycling, Journal of Engineering Materials and Technology, 122, pp. 203–209 (2000).
53. M. Omiya, K. Kishimoto, and W.M. Yang, Interface debonding model and it's application to the mixed mode interface fracture toughness, International Journal of Damage Mechanics, 11, pp. 263–286 (2002).
54. I.S. Park and J. Yu, An X-ray study on the mechanical effects of the peel test in a Cu/Cr/polyimide system, Acta Materialia, 46, pp. 2947–2953 (1988).
55. Y.B. Park, I.S. Park, and J. Yu, Interfacial fracture energy measurements in the Cu/Cr/polyimide system, Materials Science and Engineering A: Structural Materials: Properties, Microstructure and Processing, 266, pp. 261–266 (1999).
56. Y.B. Park, I.S. Park, and J. Yu, Phase angle in the Cu/polyimide/alumina system, Materials Science and Engineering A: Structural Materials: Properties, Microstructure and Processing, 266, pp. 109–114 (1999).
57. H.-H. Yu, M.Y. He, and J.W. Hutchinson, Edge effects in thin films, Acta Materialia, 49, pp. 93–107 (2001).
58. W. Yang and L.B. Freund, Shear stress concentration near the edge of a thin film deposited in a substrate, Brown Technical Report, November 1984.
59. M. Yanaka, Y. Kato, Y. Tsukahara, and N. Takeda, Effects of temperature on the multiple cracking progress of sub-micron thick glass films deposited on a polymer substrate, Thin Solid Films, 355-356, pp. 337–342 (1999).
60. B.F. Chen, J. Hwang, G.P. Yu, and J.H. Huang, In situ observation of the cracking behavior of TiN coating on 304 stainless steel subjected to tensile strain, Thin Solid Films, 352, pp. 173–178 (1999).